Mon. Not. R. Astron. Soc. **290,** 431–438 (1997)

A thermal plume in NGC 2024

Ravi Subrahmanyan,[1,2] W. M. Goss,[3] S. T. Megeath[4] and Peter J. Barnes[5]

[1]*Raman Research Institute, Sadashivanagar, Bangalore 560 080, India*
[2]*Astronomy Institutes of the University of Bonn, Universität Bonn, Auf dem Hügel 71, D-53121 Bonn 1, Germany*
[3]*National Radio Astronomy Observatory, PO Box 0, Socorro, NM 87801, USA*
[4]*MIT Haystack Observatory, Off Route 40, Westford, MA 01886, USA*
[5]*Harvard-Smithsonian Center for Astrophysics, Cambridge, MA 02138, USA*

Accepted 1997 April 4. Received 1997 March 25; in original form 1996 August 20

ABSTRACT

We present 1-arcmin resolution radio images of the Galactic H II region NGC 2024 made at 0.33 and 10.55 GHz. These are the highest dynamic range images of the nebula to date. The peak brightness in the 0.33-GHz radio continuum image indicates that the electron temperature is 6800–7600 K. The images clarify the structure of a thermal plume that is directed north from the H II region and opposite to a unipolar *molecular* outflow found in the molecular cloud near the H II region. We report the detection of H91α recombination lines from the plume: these data confirm that the plume is blueshifted relative to the molecular cloud. Finally, we discuss the relative merits of three possible explanations for the plume: that the plume results from the blueshifted counterjet to the CO outflow; that the plume is the continuation of the champagne flow observed in the denser parts of the H II region; and that the plume is produced by the photoevaporation of molecular clumps apparent in a ^{13}CO map of the region.

Key words: H II regions – ISM: individual: NGC 2024 – ISM: jets and outflows – radio continuum: ISM – radio lines: ISM.

1 INTRODUCTION

NGC 2024 is a Galactic H II region located close to the easternmost star (ζ Orionis) in the belt of Orion. At a distance of 415 pc (Anthony-Twarog 1982), NGC 2024 is one of the closest sites of recent massive star formation; consequently, the nebula and associated molecular complex have been extensively studied at multiple wavelengths. Observations up to 1980 are summarized in Goudis (1982), and more recent data are reviewed and interpreted by Barnes et al. (1989). NGC 2024 is considered to be a blister H II region (e.g. Crutcher et al. 1986) with ionized material flowing away from an H II–molecular cloud interface. A unipolar molecular flow has been detected in CO emission (Richer et al. 1992); the source of the flow is in the associated molecular cloud and the flow is inferred to be directed away from the interface with the H II gas (Barnes et al. 1989). The CO jet appears to be directed southwards. It has been a mystery as to why the flow is unipolar: perhaps the source of the flow is near the H II–molecular cloud interface and the relatively extreme conditions in the H II region may be destroying the molecular jet on that side. However, no evidence for an interaction between a hypothetical counterjet and the H II gas has been observed to date, e.g., in the form of a disruption of the orderly champagne flow in the blister H II region.

Our earlier 330-MHz imaging of NGC 2024 detected a radio plume towards the north (Subrahmanyan 1992). We present herein improved high-dynamic-range imaging of this plume at 330 MHz and 10.55 GHz that clarifies the radio structure and emission mechanism of the plume plasma. We also report detection of H91α recombination lines from the plume that throws light on the orientation of the plume vis-a-vis the overall geometry of the region. The cause for the northerly-directed plume – as well as its possible relationship to nearby molecular clumps, to the southerly-directed unipolar molecular flow and to the northerly-directed champagne flow in the blister H II region – is discussed.

2 OBSERVATIONS

2.1 330-MHz imaging observations with the VLA

NGC 2024 was observed with the Very Large Array (VLA; Napier, Thompson & Ekers 1983) in its C and D array

configurations; an integration time of 3 h was obtained in 1992 September in the D array and 2.5 h in 1993 July in the C array. The observations were made in a pair of bands 3.125-MHz wide centred at 327.5 and 333.0 MHz. The array elemental complex gains were calibrated by half-hourly observations of the unresolved source 0433 + 295. The absolute flux-density scale was determined by observations of 3C 48, the flux density of which was assumed to be 44.72 and 44.26 Jy, respectively, at the frequencies 327.5 and 333.0 MHz based on the BJPW scale (Baars et al. 1977). Observations of 3C 48 with the VLA (Perley & Crane 1986) have shown that the formula in Baars et al. gives values for the flux density at 330 MHz with an accuracy of 2 per cent.

The data were calibrated using the standard AIPS routines and self-calibrated and imaged using the 3D-imaging routines in SDE implemented by T. J. Cornwell. The 330-MHz image of NGC 2024, made with a beam of full width at half maximum (FWHM) 65.1 × 64.6 arcsec^2 at a position angle 61°.2, is shown in Fig. 1. The total flux density at 330 MHz, estimated by integrating the emission over the entire source, is 37 Jy; the peak flux density at this resolution is 2.47 Jy beam^{-1}. Details in the radio plume extending northwards from the nebula are shown separately in Fig. 2 with the same resolution.

The observation confirms the existence of the plume discovered previously by Subrahmanyan (1992). Because NGC 2024 has a low declination of about −2°, the VLA visibility tracks on the u, v plane run nearly along lines of constant v. Consequently, the synthetic beam has dominant sidelobes along the north–south line passing through the main lobe. The resultant limitation to the dynamic range for features located along the north–south line through the emission

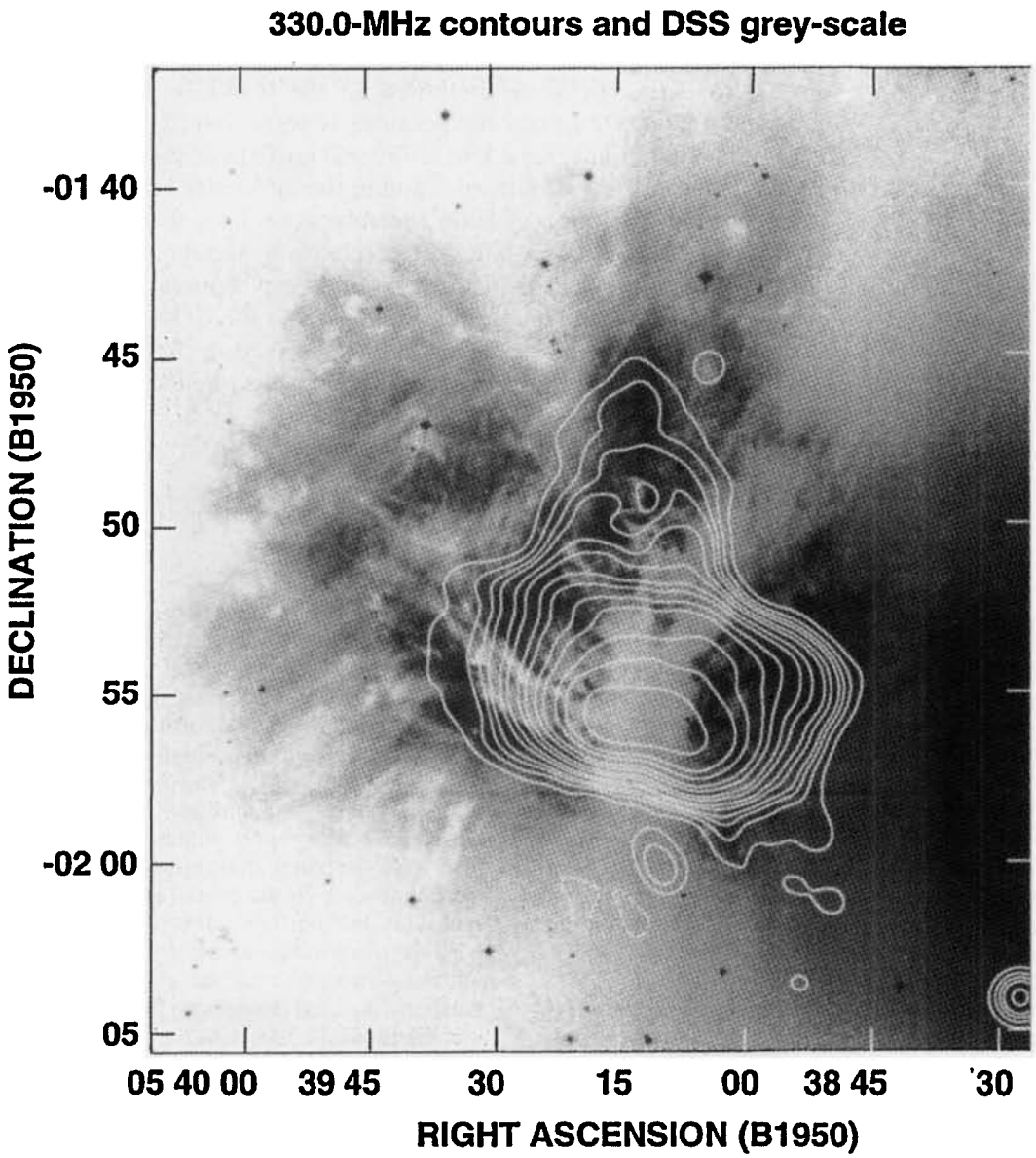

Figure 1. Contour representation of the 330-MHz image of NGC 2024 made with a beam of FWHM 65.1 × 64.6 arcsec^2 at a position angle (PA) of 61°.2. Contours are at 10 mJy beam^{-1} × (−2, 2, 4, 6, 8, 12, 16, 24, 32, 48, 64, 96, 128, 192). An optical image of NGC 2024 is shown in grey-scales.

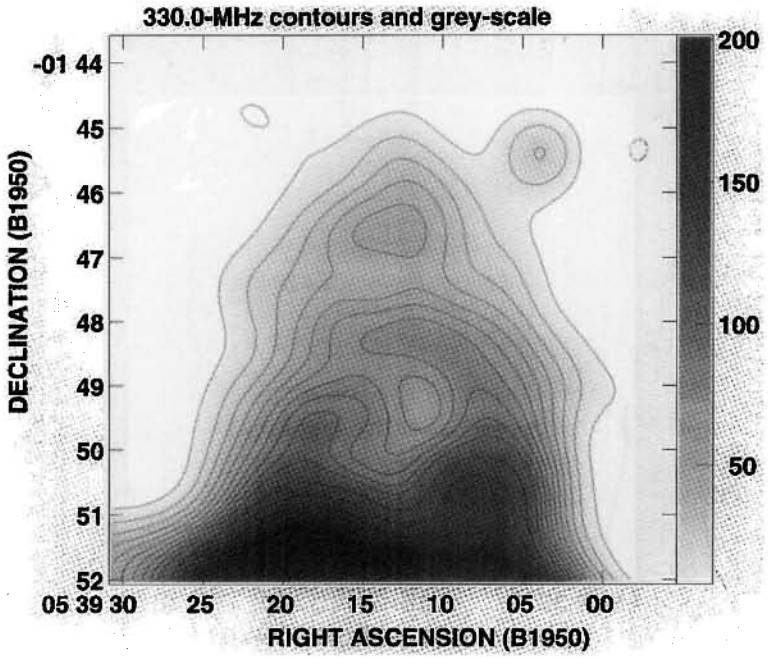

Figure 2. The radio plume of NGC 2024 at 330 MHz. The beam is the same as in the radio image of Fig. 1. Contours are at 10 mJy beam^{-1} × (− 1, 1, 2, 3, 4, 5, 6, 7, 8, 9, 10, 12, 14, 16, 20). The grey-scale range is from 10 to 200 mJy beam^{-1}.

peak may be ameliorated by increasing the hour-angle coverage: this has been our motivation for the present VLA observations. The rms noise in source-free regions of the image shown in Fig. 1 is 4 mJy beam^{-1} as compared to 11 mJy beam^{-1} for the image presented in Subrahmanyan (1992); the dynamic range of the present image improves upon that presented in Subrahmanyan (1992) by at least a factor of two, and the present image clarifies the structure in the plume.

2.2 10.55-GHz imaging observations with the Effelsberg telescope

NGC 2024 was imaged using the four-feed 10.55-GHz receiver system (Schmidt et al. 1993) on the Effelsberg 100-m telescope in 1994 August. The four beams are separated only in azimuth, and an area 30 × 30 arcmin^2 centred on NGC 2024 was scanned by moving the telescope in azimuthal direction and observing the field row by row. Two complete scans of the field were made, the field rotated through about 20° in parallactic angle during each complete scan and the two scans differ in their mean parallactic angles by about 20°. The relative horn gains and the telescope pointing were determined by observing the unresolved source 3C 286 in a similar raster-scanning mode.

Only difference measurements between horn pairs were used to reconstruct the source image; this cancels out atmospheric effects (Emerson, Klein & Haslam 1979). The image was deconvolved using a model beam pattern that was obtained as the average of two beams made with position angles equal to the mean parallactic angles of the two scans. After deconvolution, we expect features in the vicinity of the plume to be reliable at a level down to 0.4 per cent of the peak. It may be noted here that the first side lobe responses of the beam are − 17 dB below the main lobe and consequently imaging with dynamic ranges $\gtrsim$50 would require deconvolution. A previous image of NGC 2024 made with a 10.7-GHz multibeam system at Effelsberg by Gopal-Krishna et al. (1988) was not deconvolved and consequently all features displayed at levels $\lesssim$2 per cent of the peak may not be genuine; this explains why our image made at a similar frequency and resolution is dissimilar at these intensity levels (< 2 per cent). The flux-density scale was set to that of Baars et al. (1977), using the scans over the calibrator 3C 286 whose flux density was adopted to be 4.45 Jy at 10.55 GHz (Ott et al. 1994).

The image of NGC 2024 at 10.55 GHz, made with a beam of 74 arcsec FWHM, is shown in Fig. 3. The image of the radio plume at 10.55 GHz is shown separately in Fig. 4 at the same resolution. We estimate the flux scale in these images to have $\lesssim$7 per cent errors and the positional accuracy to be within 10 arcsec. The total flux density of NGC 2024 at 10.55 GHz is estimated to be 53 Jy and the peak intensity in the image is 10 Jy beam^{-1}.

2.3 Observations of H91α recombination lines from the plume

We have used the 8.6-GHz receivers on the Effelsberg 100-m telescope in 1994 September to search for H91α recombination lines from the plume. Observations were made in dual polarizations with 512 spectral channels covering 12.5-MHz bands centred at the frequency where the 8584.821-MHz transitions were observable at 0 km s^{-1} with respect to the local standard of rest (LSR). The bandpasses were calibrated by beam-switching with a throw of 20 arcmin in azimuth (more than twice the extent of the NGC 2024 nebula). The subreflector position was switched along the telescope axis by $\pm\lambda/8$ (where λ is the observing wavelength) with a period twice the beam-switching period, in

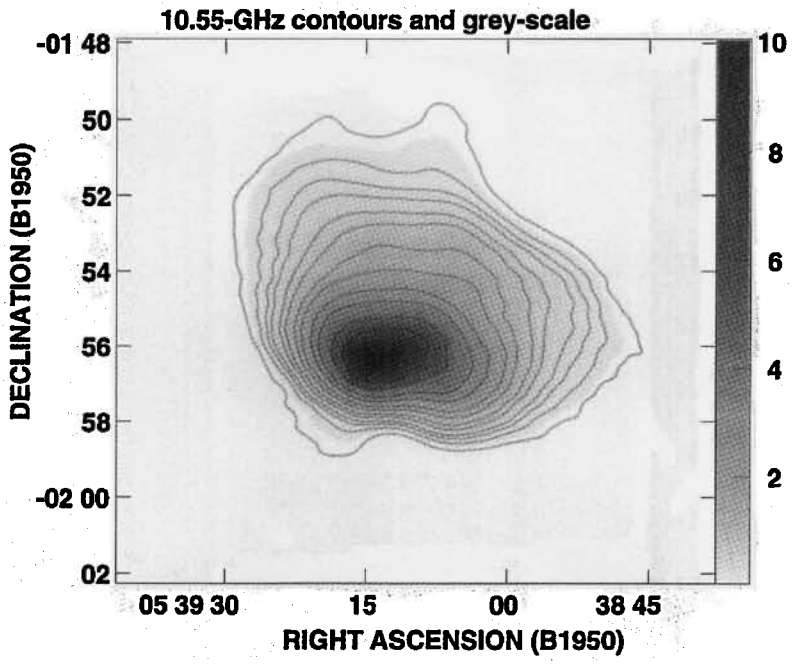

Figure 3. Image of NGC 2024 at 10.55 GHz made with a circular beam of FWHM 74 arcsec. Contours are at 0.1 Jy beam^{-1} × (1, 2, 3, 4, 6, 8, 12, 16, 24, 32, 48, 64, 96). The grey-scale range is from 0.1 to 10 Jy beam^{-1}.

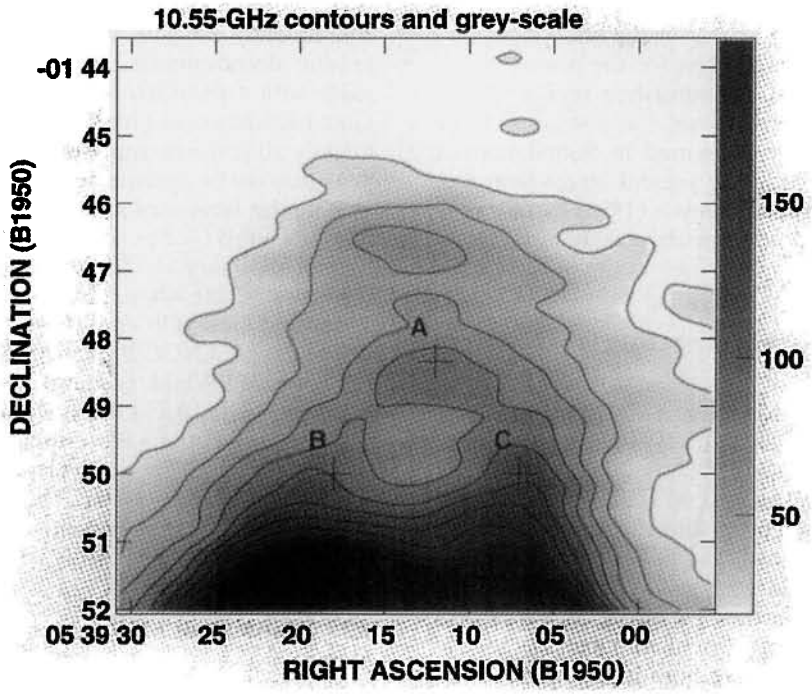

Figure 4. The radio plume of NGC 2024 at 10.55 GHz. The beam is the same as in the radio image of Fig. 3. Contours are at 20 mJy beam^{-1} × (1, 2, 3, 4, 5, 6, 7, 8, 9, 10). The grey-scale range is from 20 to 200 mJy beam^{-1}. The positions towards which recombination-line observations were made (Table 1) are marked A, B and C.

order to cancel the ripples produced in the bandpass due to standing waves in the telescope optics. The telescope pointing was periodically corrected by cross-scans over unresolved calibrators, 3C 120 and 3C 161, that were at similar azimuth/elevations.

The observed spectra are shown in Fig. 5 and the estimated line parameters are summarized in Table 1; the observations were made with a beam of 1.1 arcmin FWHM. We first observed the H91α recombination line towards position D close to the continuum peak. The line parameters were consistent with the H76α-line observations of Krügel et al. (1982) made with a beam of 1 arcmin FWHM; they observed lines with widths 22–24 km s^{-1} and LSR velocities 6–7 km s^{-1} in the vicinity of positon D. Moreover,

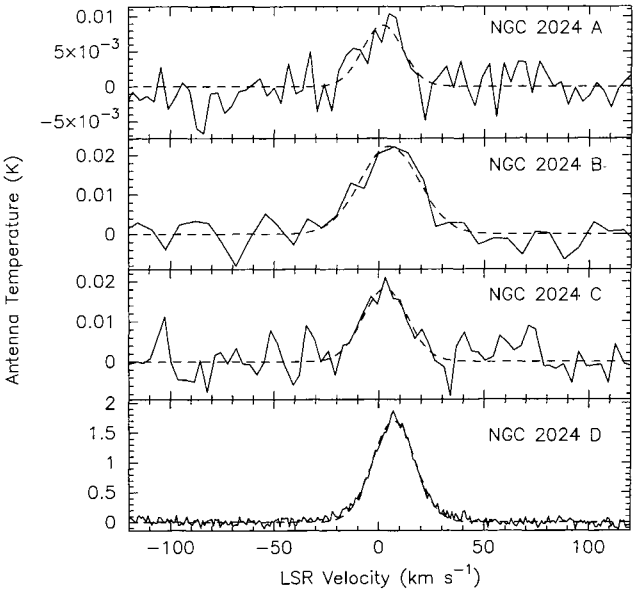

Fig. 5. H91α recombination-line spectra observed towards positions A, B and C in the plume and towards position D close to the continuum peak of NGC 2024. The dashed lines show the best-fitting Gaussian profiles.

Table 1. H91α recombination-line parameters observed towards four positions.

	RA(J2000)	DEC(J2000)	Line width (km s^{-1})	LSR velocity (km s^{-1})	Peak line flux density (Jy beam^{-1})
A	05 39 12	−01 48 20	23	+2	0.004
B	05 39 18	−01 50 00	33	+5	0.01
C	05 39 07	−01 50 00	25	+3	0.01
D	05 39 15	−01 56 00	25	+7	0.74

Krügel et al. observe the line-to-continuum ratio to be 0.17 at 15 GHz and when this value is scaled by a factor $(8.6/15.0)^{1.1}$ to get the expected ratio at 8.6 GHz, assuming local thermodynamic equilibrium, we get a value of 0.09 that is the same as the line-to-continuum ratio in our observations. Spectra were observed at three positions in the plume: A, which is the northernmost position at which we detect the line, and B and C which are at the base of the plume. The recombination-line observations made previously towards NGC 2024 (Krügel et al. 1982) did not extend this far north from the main body of the nebula. Krügel et al. had found a systematic velocity gradient across the H II region: the LSR velocity in the ionized flow varied from about +9 km s^{-1} in the south-east to about 0 km s^{-1} in the north. Farther north, in the plume, we observe LSR velocities +2 to +5 km s^{-1}: these are similar to the velocities observed by Krügel et al. in the northern parts of the main body of NGC 2024.

While observing with the Effelsberg telescope beam towards the position of the plume, where the emission intensity is about a factor of 100 lower than that towards the emission peak of NGC 2024, the spectra will be contaminated by line emission (from the vicinity of the continuum peak of the nebula) that will leak in through the beam sidelobes. However, the sidelobes at the plume distance are less than 1 per cent of the main lobe and therefore the contamination is not expected to be significant. Moreover, any contamination would be centred at about +7 km s^{-1} LSR velocity and may be expected to bias the inferred LSR velocities of the plume material towards higher values. These considerations lead us to consider the derived velocities towards A, B and C (Table 1) as strictly upper limits to the true LSR velocities of the plume gas towards those positions.

3 A COMPARISON BETWEEN THE RADIO CONTINUUM IMAGES

We have compared the 0.33- and 10.55-GHz images with an arcmin-resolution image created from the 1.67-GHz visibility data obtained by Barnes et al. (1989).

At 0.33 GHz the continuum intensity appears saturated towards the central parts, presumably because of thermal self-absorption at the lower frequency towards the regions with the higher emission measure (*EM*). The northern plume appears remarkably similar at 0.33 and 10.55 GHz; the two images have been observed with dissimilar telescopes and techniques and the agreement demonstrates that the observed morphology is real. We smoothed the 0.33- and 10.55-GHz images to a common resolution of 1.5 arcmin and computed the spectral index distribution over NGC 2024. The spectral index α (defined as $S_\nu \sim \nu^\alpha$) is in the range 0–0.4 over the southern parts of the nebula where the emissivity, and consequently the *EM*, is highest. Towards the northern parts of the main body of NGC 2024 and towards almost the entire plume at the north of the nebula, the spectral index $\alpha = 0 - 0.1$ indicating thermal emisson that is optically thin even at 330 MHz.

We have compared the intensities towards the continuum peak at 0.33 and 10.55 GHz at a resolution of 74.2 arcsec FWHM. Assuming the nebula to be optically thin at the higher frequency and that the electron temperature is a constant along the line of sight we infer $EM = 7 \times 10^5$ pc cm^6, $T_e = 6100 \pm 100$ K and that the optical depth towards the peak is 4.8 ± 0.4 at 0.33 GHz (see Subrahmanyan & Goss 1996 for the method).

At arcmin resolution, the main body of NGC 2024 has the same appearance at 1.67 and 10.55 GHz. At a resolution of 74.2 arcsec, the flux density towards the continuum peak is 10.7 Jy beam^{-1} at 1.67 GHz as compared to 10.0 Jy beam^{-1} at 10.55 GHz. Allowing for the errors expected in the absolute scale of the 10.55-GHz image, the *EM* and T_e values estimated above are consistent with the relative flux densities at 1.67 and 10.55 GHz; the optical depth towards the continuum peak at 1.67 GHz exceeds 0.1.

The peak flux density in the 0.33 GHz image in Fig. 1 corresponds to a beam-averaged brightness temperature of 6600 K. We have smoothed this image to progressively poorer resolutions and obtained the variation in the beam-averaged brightness with the FWHM of the beam. Modelling the source intensity to have top-hat or Gaussian distributions, we infer that the above variations imply a source with peak brightness in the range 6700–7500 K. Correcting for the effects of finite optical depth and background brightness (see Subrahmanyan 1992 and Subrahmanyan & Goss 1995 for procedural details), the 0.33-GHz radio continuum image implies that $T_e = 6800$–7600 K. This T_e estimate, based on radio continuum imaging, is consistent with previous estimates of T_e based on radio recombination line

observations: Krügel et al. (1982) estimate $T_e = 7000$–8000 K from their H76α line-to-continuum ratios.

4 THE ORIGIN OF THE PLUME

The plume consists of a pair of loops that appear to emerge from the main body of the nebula and possibly connect to form a 'hollow shell' or 'bubble' structure with a diameter of about 0.3 pc. Farther north there is a distinct emission peak, and both of these features are apparently embedded in more diffuse thermal gas. The plume is seen to extend up to 0.7 pc (6 arcmin) out of the main nebula.

We reproduce an optical image of NGC 2024 extracted from the digitized archives of the SERC IIIaJ southern sky survey plates in Fig. 1 in grey-scale, with the 330-MHz radio-continuum contours superposed. The plume is apparent in the optical image and is bounded on the east and west sides by dust lanes, which give the appearance that the plume is partially obscured and that its narrow width may only be an illusion owing to obscuring foreground dust. However, the 330 MHz image is not affected by extinction and clearly shows that the plume is a narrow enhancement in the electron density.

4.1 A continuation of the champagne flow?

NGC 2024 has been modelled as a blister H II region by many authors (e.g. Grasdalen 1974; Krügel et al. 1982; Crutcher et al. 1986; Barnes et al. 1989). In this model, the exciting stars forming the H II gas are postulated as initially embedded in, but close to the boundary of, the parent neutral molecular cloud. Density gradients and anisotropy in the environment are expected to have culminated in a 'champagne' flow of the high-pressured ionized gas towards the interclump region (e.g. Tenorio-Tagle 1982). The geometry postulated for NGC 2024 envisages an exciting star initially embedded in the near side of a molecular cloud. Subsequently, the H II gas has broken through the cloud on the near side and the thermal plasma, observed in its thermal bremsstrahlung emission as the main body of the radio nebula, is flowing northwards and towards the Sun. This flow was studied by Krügel et al. (1982), who, using recombination line measurements, observed that the thermal gas is accelerated from its local rest velocity of about $+9$ km s^{-1}, northwards and towards the Sun; and LSR velocity of about 0 km s^{-1} was observed by Krügel et al. at the northern rim. As the ionized gas expands into the low-density interclump region, the density of the gas decreases. The sensitivity of our radio continuum observations corresponds to a detection limit of about $EM = 10^3$ pc cm^6 assuming a thermal plasma with an electron temperature of 10^4 K. Thus, the optical nebula, which extends beyond the boundary of the observed radio emission, can be understood as the low-density, outer end of the flow which is not detectable by our radio observations.

In the context of this model, we attribute the plume to the low-density outer region of the champagne flow. The observed recombination-line velocities in the plume are comparable to those measured by Krügel et al. (1982) in the adjoining northern edge of the nebula. Consequently, although we do not detect an *acceleration* of the plume gas relative to the outer parts of the H II region, there is a similarity in velocities which suggests that the plume is a continuation of the champagne flow. However, the champagne-flow model makes it difficult to explain two features of the plume: first, the plume has a much narrower spatial width than the main body of the H II region, secondly, north–south profiles of the intensity at 10.55 GHz indicate a discontinuity in the gradient of the intensity profile, and consequently in *EM*, at the base of the plume. These argue in favour of models in which the plume is a distinct structure and not simply an extension of the champagne flow.

4.2 A counterjet of the unipolar CO jet?

The velocity distribution image in H76α radio recombination lines made by Krügel et al. (1982) shows marginal evidence for a channel of higher-velocity thermal gas flowing north within the main body of NGC 2024; this channel may be traced to the region of the base of the plume. Subrahmanyan (1992) has suggested that the plume may be the counterjet to a unipolar molecular outflow located in the dense gas at the southern edge of the nebula. Richer et al. (1992) and Chernin (1996) have detected a north-to-south, *unipolar* (i.e. redshifted only) flow of CO gas in the molecular cloud associated with NGC 2024. The source of the flow is believed to be close to RA $= 05^h39^m12^s.6$, Dec. $= -01°57'$, south of the peak in the radio continuum (Barnes & Crutcher 1990). The unipolar jet is directed south and is redshifted, indicating that the flow is directed into the neutral gas and away from the H II–molecular cloud interface. It may be noted here that the initial detection of a molecular counterjet, i.e. a blueshifted jet, by Sanders & Willner (1985) has not been substantiated by the subsequent observations of Richer and Chernin. One explanation for the unipolar flow is that the outflow centre lies close to the ionization front; consequently, any blueshifted counterpart may be stopped or ionized at the interface resulting in the absence of blueshifted CO emission. The outflow may then accelerate a jet of ionized gas, resulting in higher velocity material emerging from the northern end of the champagne flow.

The parent molecular cloud is at an LSR velocity of $+11.2$ km s^{-1} (Richer et al. 1992) and the thermal gas towards the continuum peak of NGC 2024 is at about $+7$ km s^{-1}. Our recombination line measurements of the LSR velocity towards the plume (Table 1), even if viewed as upper limits, confirm that the plume gas is blueshifted relative to the molecular cloud and support the counterjet model. Using the observed plume gas velocity, we can determine the momentum and energy of the plume. We estimate the flux density from the plume to be about 1.3 Jy at 330 MHz and 0.9 Jy at 10.55 GHz. We model the plume as an H II region with a diameter 0.5 pc and length 0.7 pc and assume that the thermal plume material has an electron temperature of 8000 K. The plume is derived to have an emission measure of 10^4 pc cm^{-6}. The electron density is derived to be $10^2 f^{-1/2}$ cm^{-3} and the total mass of thermally emitting gas is estimated to be about $0.5 f^{1/2}$ M$_\odot$, where f is the volume filling factor. Assuming that this thermal plume material has a velocity of 9 km s^{-1} (with respect to the $+11.2$ km s^{-1} local rest velocity), we obtain the plume momentum to be $5 f^{1/2}$ M$_\odot$ km s^{-1} and the bulk kinetic energy to be $0.5 \times 10^{38} f^{1/2}$ J. These values have been derived

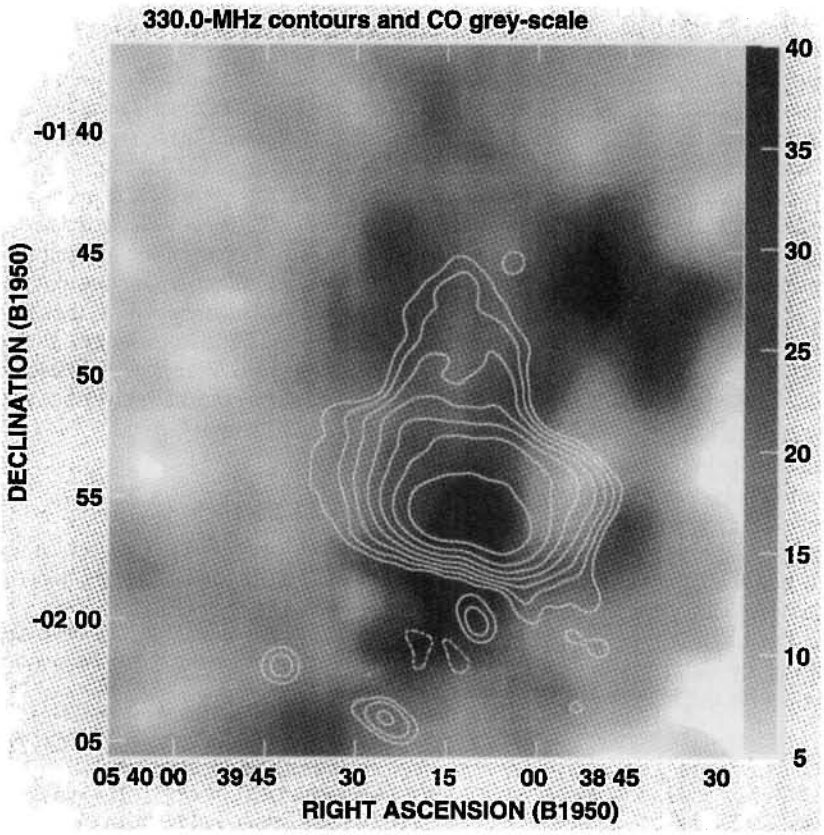

Figure 6. Contour representation of the 330-MHz radio continuum image of NGC 2024, with the same beam as in Fig. 1, overlaid on a grey-scale representation of a ^{13}CO integrated-intensity image. Contours are at 10 mJy beam^{-1} × (−2, 2, 4, 8, 16, 32, 64, 128). Grey-scales in the range 5 to 40 K km s^{-1}

for the part of the plume observed beyond the edge of the main body of NGC 2024. If the plume is a feature distinct from the champagne flow and originates at the origin of the southern CO jet, we may expect the total mass and energy in this thermal flow to be a factor 2–3 higher than the above estimates. The mass/energy in the thermal flow is then comparable with the parameters derived for the southern CO jet (tabulated in Richer et al. 1992) and is consistent with the interpretation of the plume as the CO counterjet. We may note that this comparison is not affected by the inclination of the jet relative to the plane of the sky since we expect that the ionized and molecular jet will have similar inclinations.

4.3 The role of molecular clumps adjoining the plume

Comparison of the 330-MHz image with a ^{13}CO image of the region (J. Bally, private communication) suggests an alternative scenario. The ^{13}CO integrated-intensity image is reproduced as a grey-scale in Fig. 6 with 330-MHz contours superposed. The CO image indicates that the plume is bounded on the east and west sides by molecular clumps. There appears to be a steep decrease in 330-MHz intensity at points where the H II region meets the molecular clumps, suggesting that the H II is in part ionization bounded by the clumps. In this case, the clumps may block part of the champagne flow, resulting in the collimation of the outflowing gas and the resulting plume. Although this model explains why the plume is narrow, it fails to explain the discontinuity in the gradient of the intensity profile at the base of the plume: we would expect, in a champagne flow, that the density should smoothly drop with distance from the compact centre of the H II region.

Alternatively, the plume may arise from the photoevaporation, either directly or through diffuse illumination, of the molecular clumps. The ionized gas would then flow into the lower density, interclump medium. Given the distance of the exciting star(s) from the clumps, we would expect the ionization rate of the clumps, and thus the density of the associated ionized gas, to be substantially lower than the densities found towards the compact H II region. Thus, this model accounts for the low intensity of the plume. Additionally, the morphology of the 330-MHz emission shows that the boundaries of the plume adjoining the clumps are edge-brightened and this is consistent with the hypothesis that the ionized gas is expanding as it flows from the clump surfaces into a lower density medium.

The weakness of the photoevaporation scenario is that it does not correctly predict the velocity of the plume gas. Because the clumps obscure the nebula in the optical image (Fig. 1), we expect that the clumps are in the foreground relative to the H II region. Accordingly, the photoevaporation model predicts that the photoevaporating gas would flow, in part, towards the ionizing star and the compact H II

region. Consequently, the LSR velocity of the plume material should either be the same as that of the clumps or redshifted. The ^{13}CO data shows that the molecular gas bounding the plume has a velocity range of 5–15 km s^{-1}; therefore, the velocities measured towards the plume (2–5 km s^{-1}) are inconsistent with the photoevaporation model. We may, however, note that the clump velocities fall within the broad linewidths ($\sim$25 km s^{-1}) of the recombination lines; hence, we cannot categorically reject this hypothesis on the basis of this inconsistency.

4.4 Discussion

Comparing the scenarios considered above, we conjecture that the counterjet model is probably the most viable candidate due to its simplicity and the lack of inconsistencies with our current data set; however, a convincing test to distinguish the three models is not available. We suggest that IR spectroscopy and narrow-band imaging may be useful in studying the structure and velocity of the plume with a higher spatial resolution. The resulting data could test the three proposed explanations by determining whether the plume is indeed interacting with the neighbouring molecular clumps.

5 SUMMARY

We have presented arcmin resolution images of NGC 2024 that clarify the structure in a plume directed north from the centre of the H II region: the two images consistently show that the plume has a bubble-like or loop structure at the base. The plume is shown to be composed of thermal plasma that is optically thin at 330 MHz and is being seen in thermal bremsstrahlung emission. Detection of radio recombination lines from the plume indicates that the plasma has an LSR velocity similar to that in the northern parts of the main body of the radio nebula and is blueshifted with respect to the molecular cloud. The evidence indicates that the plume most likely originates as a northward flowing counterjet of the unipolar molecular jet observed to be directed southwards in the associated molecular cloud; the northward flow of the beam, which is ionized in the H II region, may be channeled by the local molecular clumps.

We derive the electron temperature towards the centre of the NGC 2024 thermal nebula to be 6800–7600 K from the peak brightness in the 330-MHz radio continuum image.

ACKNOWLEDGMENTS

The National Radio Astronomy Observatory is a facility of the National Science Foundation operated under cooperative agreement by Associated Universities, Inc. We thank R. Wielebinski for his support, T. L. Wilson, K.-H. Mack and Wilfred Walsh for assistance with the Effelsberg observing, Patricia Reich for assistance with the NOD2 software, Tim Cornwell for his help in using the SDE software and Ralph Gaume for his comments. RS acknowledges financial assistance from the Forschungszentrum Jülich GmbH. STM acknowledges the support of a fellowship from the Max Planck Gesselleschaft during his stay at the Max-Planck-Institut für Radioastronomie, where much of this work was performed.

REFERENCES

Anthony-Twarog B. J., 1982, AJ, 87, 1213
Baars J. W. M., Genzel R., Pauliny-Toth I. I. K., Witzel A., 1977, A&A, 61, 99
Barnes P. J., Crutcher R. M., 1990, ApJ, 351, 176
Barnes P. J., Crutcher R. M., Bieging J. H., Storey J. W. V., Willner S. P., 1989, ApJ, 342, 883
Chernin L. M., 1996, ApJ, 460, 711
Crutcher R. M., Henkel C., Wilson T. L., Johnston K. J., Bieging J. H., 1986, ApJ, 307, 302
Emerson D. T., Klein U., Haslam C. G. T., 1979, A&A, 76, 92
Gopal-Krishna, Subrahmanyan R., Swarup G., Thum C., Steppe H., 1988, Vistas Astron., 31, 207
Goudis C., 1982, The Orion Complex: A case study of interstellar matter, Ap&SS Lib., 90, p. 211
Grasdalen G. L., 1974, ApJ, 193, 373
Krügel E., Thum C., Martin-Pintado J., Pankonin V., 1982, A&AS, 48, 345
Napier P. J., Thompson A. R., Ekers R. D., 1983, Proc. IEEE, 71, 1295
Ott M., Witzel A., Quirrenbach A., Krichbaum T. P., Standke K. J., Schalinski C. J., Hummel C. A., 1994, A&A, 284, 331
Perley R., Crane P., 1986, NRAO Newsletter, 27, 9
Richer J. S., Hills R. E., Padman R., Russell A. P. G., 1992, MNRAS, 254, 525
Sanders D. B., Willner S. P., 1985, ApJ, 293, L39
Schmidt A., Wongsowijoto S., Lochner O., Reich W., Reich P., Fürst E., Wielebinski R., 1993, Technischer Bericht des MPIfR, Bonn, No. 73
Subrahmanyan R., 1992, MNRAS, 254, 719
Subrahmanyan R., Goss W. M., 1995, MNRAS, 275, 755
Subrahmanyan R., Goss W. M., 1996, MNRAS, 281, 239
Tenorio-Tagle G., 1982, in Roger R. S., Dewdney P. E., eds, Regions of Recent Star Formation. Ap&SS Lib., 93, p. 1